RSC Advances

Supplementary Information

Direct synthesis and characterization of mixed-valent $Li_{0.5-\delta}CoPO_4$, a Li-deficient derivative of the *Cmcm* polymorph of $LiCoPO_4$

Jennifer Ludwig,[a] Carlos Alarcón-Suesca,[a] Stephan Geprägs,[b] Dennis Nordlund,[c] Marca M. Doeff,[d] Inés Puente Orench,[e,f] and Tom Nilges[a]*

[a.] *Technical University of Munich, Department of Chemistry, Synthesis and Characterization of Innovative Materials, Lichtenbergstr. 4, 85747 Garching, Germany*
[b.] *Walther Meissner Institute, Bavarian Academy of Sciences and Humanities, Walther-Meissner-Str. 8, 85747 Garching, Germany*
[c.] *Stanford Synchrotron Radiation Lightsource, SLAC National Accelerator Laboratory, 2575 Sand Hill Rd, Menlo Park, CA, 94025, USA*
[d.] *Lawrence Berkeley National Laboratory, Energy Storage and Distributed Resources Division, 1 Cyclotron Rd, Berkeley, CA, 94720, USA*
[e.] *Instituto de Ciencia de Materiales de Aragón, Pedro Cerbuna 12, 50009 Zaragoza, Spain*
[f.] *Institut Laue-Langevin, 71 avenue des Martyrs, B.P. 156, 38042 Grenoble Cedex 9, France*
* Corresponding author. E-mail: tom.nilges@lrz.tum.de, Tel.: +49 89 289 13110, Fax: +49 89 289 13762

Note

The following crystal structure datasets were used as starting models for all Rietveld refinements presented in this material:
$LiCoPO_4$ (*Cmcm*, $Z = 4$, ICSD no. 432186, see ref. [1])
$LiCoPO_4$ (*Pnma*, $Z = 4$, ICSD no. 431999, see ref. [2])
α-$Co_2P_2O_7$ ($P2_1/c$, Z = 4, ICSD no. 280959, see ref. [3])

For details on the refinements, please refer to the experimental part in the main article.

1 Detailed comparison of the X-ray powder diffraction patterns of $Li_{0.5-\delta}CoPO_4$ (*Cmcm*) and $Li_{1-\gamma}CoPO_4$ (*Cmcm*)

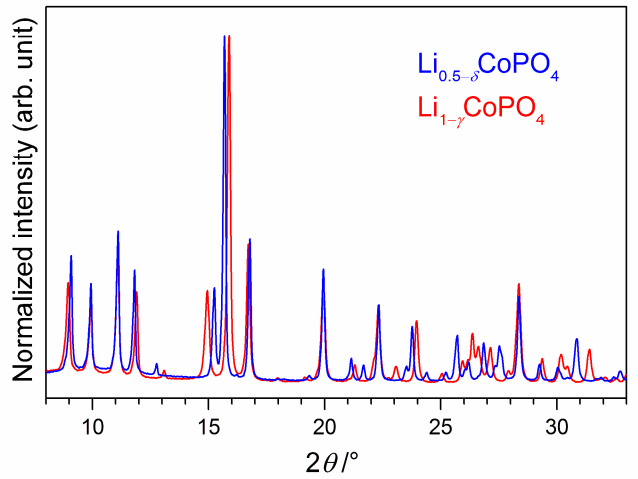

Figure S1 Comparison of the X-ray powder diffraction patterns (transmission geometry, Mo $K_{\alpha1}$ radiation, measurement time: 12 h; displayed with normalized intensities for better comparison) of $Li_{0.5-\delta}CoPO_4$ (*Cmcm*, blue) and (b) $Li_{1-\gamma}CoPO_4$ (*Cmcm*, red) in the 2θ region of 25.5–27.5°. While the pattern of $Li_{0.5-\delta}CoPO_4$ appears to be roughly similar to the one of $LiCoPO_4$, indicating that the crystal structures are strongly correlated, some significant differences can be recognized. The (100) reflection at ~8.9° 2θ is shifted towards higher angles for $Li_{0.5-\delta}CoPO_4$, whereas the (021) and (002) reflections at ~11.9° and ~13.1° are shifted to larger values. A similar trend is observed for the (200) and (112) reflections at 15.0° and 15.9°, resulting in a narrowing of the two reflections. Furthermore, completely different peak patterns can be observed in the 2θ region of 25.5–27.5°. The described shifts are mainly related to changes in the cell dimensions.

2 Rietveld refinement details of $Li_{0.5-\delta}CoPO_4$ (*Cmcm*) and $Li_{1-\gamma}CoPO_4$ (*Cmcm*) based on X-ray powder diffraction data

Table S1 Crystallographic parameters of $Li_{0.5-\delta}CoPO_4$ and $Li_{1-\gamma}CoPO_4$ (both *Cmcm*, $Z = 4$) as refined from X-ray powder diffraction data ($T = 298$ K): (a,c) refinement with fixed Li and Co site occupancy factors (δ, $\gamma = 0$) compared to (b,d) the free refinement of the Li and Co occupancies ($\delta = 0.11(2)$, $\gamma = 0.06(2)$; *cf.* Table 1 in the main article) [a]

Empirical formula	**a) $Li_{0.5}CoPO_4$**	**b) $Li_{0.39(2)}Co_{0.96(1)}PO_4$**	**c) $LiCoPO_4$**	**d) $Li_{0.94(2)}Co_{0.96(1)}PO_4$**
M_r (g·mol^{-1})	157.4	154.3	160.8	158.1
Crystal system	orthorhombic	orthorhombic	orthorhombic	orthorhombic
Space group (No.)	*Cmcm* (63)	*Cmcm* (63)	*Cmcm* (63)	*Cmcm* (63)
Z	4	4	4	4
a (Å)	5.3386(2)	5.3385(2)	5.4433(3)	5.4432(3)
b (Å)	8.1763(4)	8.1763(3)	8.1694(4)	8.1695(4)
c (Å)	6.3714(3)	6.3716(2)	6.2128(3)	6.2128(3)
V (Å^3)	278.11(2)	278.116(19)	276.28(2)	276.28(2)
F(000)	302	297	308	302
ρ (calcd.) (g·cm^{-3})	3.759(1)	3.684(1)	3.867(1)	3.800(1)
R_p	0.0271	0.0257	0.0209	0.0196
R_{wp}	0.0347	0.0327	0.0272	0.0255
R_{exp}	0.0267	0.0267	0.0252	0.0252
R_F	0.0165	0.0143	0.0128	0.0106
R_B	0.0283	0.0254	0.0214	0.0184
χ^2	1.30	1.23	1.08	1.01
Data/restraints/ parameter	3800/0/57	3800/0/59	3835/0/55	3835/0/57

[a] The estimated standard deviations were calculated by the Berar's procedure and are indicated in parentheses.

Table S2 Fractional atomic coordinates and isotropic thermal displacement parameters of $Li_{0.5-\delta}CoPO_4$ and $Li_{1-\gamma}CoPO_4$ (both *Cmcm*, *Z* = 4) as refined from X-ray powder diffraction data (*T* = 298 K): (a,c) refinement with fixed Li and Co site occupancy factors (δ, γ = 0) compared to (b,d) the free refinement of the Li and Co occupancies (δ = 0.11(2), γ = 0.06(2)) [a]

Sample	Atom	Wyck. position	Occupancy	*x*/a	*y*/b	*z*/c	U_{iso} (Å^2)
a) $Li_{0.5}CoPO_4$	Li1	4*c*	0.5 [b]	0	0.675 [c]	¼	0.019 [c]
	Co1	4*a*	1	0	0	0	0.0150(7)
	P1	4*c*	1	0	0.3567(4)	¼	0.0131(9)
	O1	8*f*	1	0	0.2502(4)	0.0526(7)	0.0179(15)
	O2	8*g*	1	0.2347(6)	0.4621(5)	¼	0.0064(14)
b) $Li_{0.39(2)}Co_{0.96(1)}PO_4$	Li1	4*c*	0.39(2)	0	0.675 [c]	¼	0.019 [c]
	Co1	4*a*	0.964(5)	0	0	0	0.0133(6)
	P1	4*c*	1	0	0.3565(3)	¼	0.0152(9)
	O1	8*f*	1	0	0.2495(4)	0.0497(8)	0.0237(16)
	O2	8*g*	1	0.2355(6)	0.4633(4)	¼	0.0101(13)
c) $LiCoPO_4$	Li1	4*c*	1	0	0.675 [c]	¼	0.019 [c]
	Co1	4*a*	1	0	0	0	0.0107(5)
	P1	4*c*	1	0	0.3523(4)	¼	0.0064(8)
	O1	8*f*	1	0	0.2474(4)	0.0500(7)	0.0039(13)
	O2	8*g*	1	0.2255(6)	0.4653(5)	¼	0.0028(12)
d) $Li_{0.94(2)}Co_{0.96(1)}PO_4$	Li1	4*c*	0.94(2)	0	0.675 [c]	¼	0.019 [c]
	Co1	4*a*	0.955(5)	0	0	0	0.0091(5)
	P1	4*c*	1	0	0.3525(3)	¼	0.0097(8)
	O1	8*f*	1	0	0.2468(3)	0.0477(7)	0.0096(13)
	O2	8*g*	1	0.2273(5)	0.4667(5)	¼	0.0072(12)

[a] The estimated standard deviations were calculated by the Berar's procedure and are indicated in parentheses. [b] The occupancy of Li was kept fixed at 50% on basis of the Li contents determined by elemental analysis (see Table 2 in the main article), which indicated that $Li_{0.5-\delta}CoPO_4$ contains about half the amount of lithium compared to $Li_{1-\gamma}CoPO_4$. [c] Li positions and thermal displacement parameters have been fixed as they cannot be deduced by means of X-ray diffraction due to the low atomic scattering factor of Li.

Table S3 Selected interatomic distances of $Li_{0.5-\delta}CoPO_4$ and $Li_{1-\gamma}CoPO_4$ (both *Cmcm*, *Z* = 4) as refined from X-ray powder diffraction data (*T* = 298 K): (a,c) refinement with fixed Li and Co site occupancy factors (δ, γ = 0) compared to (b,d) the free refinement of the Li and Co occupancies (δ = 0.11(2), γ = 0.06(2)) [a]

Atom pair			Comment	*d* (Å)			
				a) $Li_{0.5}CoPO_4$	**b) $Li_{0.39(2)}Co_{0.96(1)}PO_4$**	**c) $LiCoPO_4$**	**d) $Li_{0.94(2)}Co_{0.96(1)}PO_4$**
Li1	O1	×2	[LiO_4] unit	2.022(4)	2.007(5)	1.968(4)	1.957(4)
	O2	×2	[LiO_4] unit	2.145(4)	2.140(3)	2.107(4)	2.104(3)
	Li–O average		[LiO_4] unit	2.084	2.074	2.038	2.031
	Li1	×2	[100] direction	5.3386(5)	5.3385(4)	5.4433(6)	5.4432(5)
	Co1	×2	to next layer ([010])	3.0981(2)	3.09816(19)	3.0760(2)	3.0760(2)
	Co1	×4	within *ac* layer	3.4219(2)	3.42193(18)	3.4444(2)	3.4444(2)
	Li–Co average		–	3.3140	3.3140	3.3216	3.3216
	P1	×1	[010] direction	2.602(3)	2.604(3)	2.636(3)	2.635(3)
	P1	×2	[010] direction	3.0549(15)	3.0539(14)	3.0832(14)	3.0837(13)
	Li–P average		IR spectra	2.904	2.904	2.934	2.934
Co1	O1	×2	[CoO_6] unit, to next layer ([010])	2.073(3)	2.065(3)	2.045(3)	2.038(3)
	O2	×4	[CoO_6] unit (within *ac* layer)	2.154(2)	2.150(2)	2.174(2)	2.166(2)
	Co–O average		[CoO_6] unit	2.127	2.122	2.131	2.123
	Li1	×2	to next layer ([010])	3.0981(2)	3.09816(19)	3.0760(2)	3.0760(2)
	Li1	×4	within *ac* layer	3.4219(2)	3.42193(18)	3.4444(2)	3.4444(2)
	Co–Li average		–	3.3140	3.3140	3.3216	3.3216
	Co1	×2	within *ac* layer ([001])	3.1857(3)	3.1858(2)	3.1064(3)	3.1064(3)
	Co1	×4	[010] to next layer	4.8824(3)	4.8824(3)	4.9084(4)	4.9084(3)
	Co1	×2	within *ac* layer ([100])	5.3386(5)	5.3385(4)	5.4433(6)	5.4432(5)
	Co–Co average		–	5.5723	4.5723	4.5916	4.5916
	P1	×2	to next layer ([010])	3.323(3)	3.321(3)	3.271(3)	3.272(2)
	P1	×4	within *ac* layer ([100])	3.3219(11)	3.3226(10)	3.3579(11)	3.3574(10)
	Co–P average		IR spectra	3.322	3.322	3.329	3.329
P1	O1	×2	[PO_4] unit	1.530(5)	1.547(5)	1.510(4)	1.525(4)
	O2	×2	[PO_4] unit	1.521(4)	1.531(4)	1.536(4)	1.550(4)
	P–O average		[PO_4] unit	1.526	1.539	1.523	1.538
	Li1	×1	within *ac* layer ([010])	2.602(3)	2.604(3)	2.636(3)	2.635(3)
	Li1	×2	to next layer ([010])	3.0549(15)	3.0539(14)	3.0832(14)	3.0837(13)
	P–Li average		IR spectra	2.904	2.904	2.934	2.934
	P1	×2	[100] direction	5.3386(5)	5.3385(4)	5.4433(6)	5.4432(5)
	Co1	×2	to next layer ([010])	3.323(3)	3.321(3)	3.271(3)	3.272(2)
	Co1	×4	within *ac* layer ([100])	3.3219(11)	3.3226(10)	3.3579(11)	3.3574(10)
	P–Co average		IR spectra	3.322	3.322	3.329	3.329

[a] The estimated standard deviations were calculated by the Berar's procedure and are indicated in parentheses.

3 Rietveld refinement details of $Li_{0.5-\delta}CoPO_4$ (*Cmcm*) and $Li_{1-\gamma}CoPO_4$ (*Cmcm*) based on neutron powder diffraction data

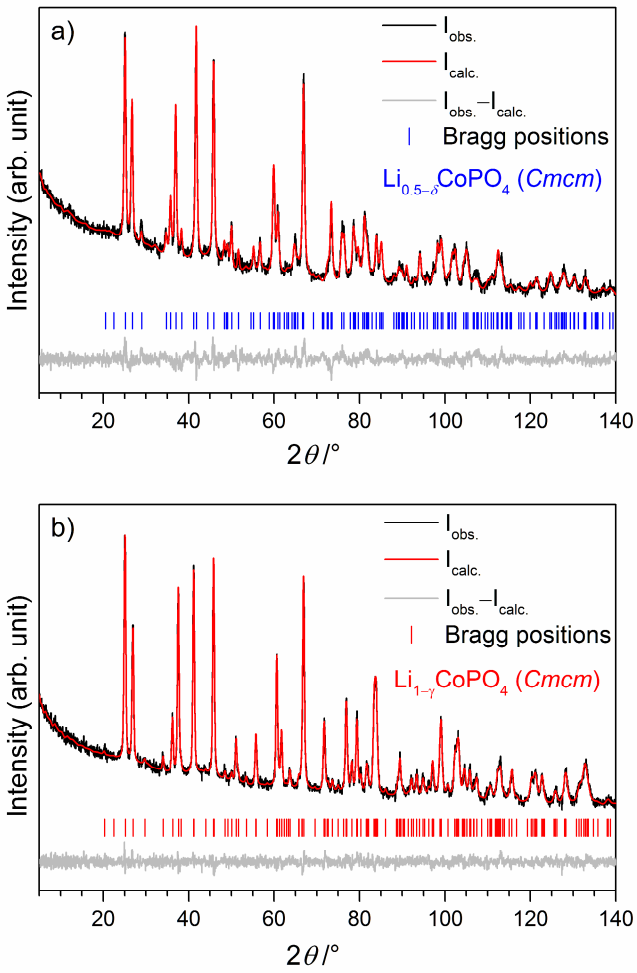

Figure S2 Rietveld fits of the neutron powder diffraction data (T = 296 K) of (a) $Li_{0.5-\delta}CoPO_4$ (*Cmcm*; refined composition: $Li_{0.37(4)}Co_{0.98(1)}PO_4$, δ = 0.13(4)), and (b) $Li_{1-\gamma}CoPO_4$ (*Cmcm*; refined composition: $Li_{0.90(2)}Co_{0.95(6)}PO_4$, γ = 0.10(2)).

Table S4 Crystallographic parameters of (a) $Li_{0.5-\delta}CoPO_4$ (δ = 0.13(4), *Cmcm*, *Z* = 4) and (b) $Li_{1-\gamma}CoPO_4$ (γ = 0.10(2), *Cmcm*, *Z* = 4) as refined from neutron powder diffraction data (*T* = 296 K) [a]

Empirical formula	**a) $Li_{0.37(4)}Co_{0.98(1)}PO_4$**	**b) $Li_{0.90(2)}Co_{0.95(6)}PO_4$**
M_r (g·mol^{-1})	154.3	157.8
Crystal system	orthorhombic	orthorhombic
Space group (No.)	*Cmcm* (63)	*Cmcm* (63)
Z	4	4
a (Å)	5.3385(2)	5.4432(0)
b (Å)	8.1763(3)	8.1695(0)
c (Å)	6.3716(2)	6.2128(0)
V (Å^3)	278.11(8)	276.27(2)
F(000)	12.99(7)	11.56(9)
ρ (calcd.) (g·cm^{-3})	3.711	3.788
R_p	0.0236	0.0237
R_{wp}	0.0299	0.0300
R_{exp}	0.0221	0.0256
R_F	0.0330	0.0207
R_B	0.052	0.0326
χ^2	1.88	1.38
Data/restraints/parameter	3200/0/14	3200/0/14

[a] The estimated standard deviations are indicated in parentheses.

Table S5 Fractional atomic coordinates and isotropic thermal displacement parameters of (a) $Li_{0.5-\delta}CoPO_4$ (δ = 0.13(4), *Cmcm*, *Z* = 4) and (b) $Li_{1-\gamma}CoPO_4$ (γ = 0.10(2), *Cmcm*, *Z* = 4) as refined from neutron powder diffraction data (*T* = 296 K) [a]

Sample	Atom	Wyck. position	Occupancy	*x*/a	*y*/b	*z*/c	U_{iso} (Å^2)
a) $Li_{0.37(4)}Co_{0.98(1)}PO_4$	Li1	4*c*	0.37(4)	0	0.543(4)	¼	0.023(10)
	Co1	4*a*	0.98(2)	0	0	0	0.006(3)
	P1	4*c*	1	0	0.3529(4)	¼	0.0094(7)
	O1	8*f*	1	0	0.2473(3)	0.0522(3)	0.0173(5)
	O2	8*g*	1	0.2365(5)	0.4629(3)	¼	0.0132(5)
b) $Li_{0.90(2)}Co_{0.95(6)}PO_4$	Li1	4*c*	0.90(3)	0	0.6760(11)	¼	0.017(3)
	Co1	4*a*	0.95(6)	0	0	0	0.0091(5)
	P1	4*c*	1	0	0.352700	¼	0.0098(9)
	O1	8*f*	1	0	0.2474(2)	0.0476(3)	0.0092(4)
	O2	8*g*	1	0.2280(4)	0.4668(2)	¼	0.0092(4)

[a] The estimated standard deviations are indicated in parentheses.

Table S6 Selected interatomic distances of (a) $Li_{0.5-\delta}CoPO_4$ (δ = 0.13(4), *Cmcm*, *Z* = 4) and (b) $Li_{1-\gamma}CoPO_4$ (γ = 0.10(2), *Cmcm*, *Z* = 4) as refined from neutron powder diffraction data (*T* = 296 K) [a]

Atom pair			*d* (Å)	
			a) $Li_{0.37(4)}Co_{0.98(1)}PO_4$	**b) $Li_{0.90(2)}Co_{0.95(6)}PO_4$**
Li1	O1	×2	2.58(2)	1.952(3)
	O2	×2	1.42(2)	2.112(8)
	Li1–O average		2.00	2.032
Co1	O1	×2	2.049(2)	2.043(2)
	O2	×4	2.1501(3)	2.163(2)
	Co1–O average		2.116	2.123
P1	O1	×2	1.528(3)	1.524(2)
	O2	×2	1.546(2)	1.552(2)
	P1–O average		1.537	1.538

[a] The estimated standard deviations are indicated in parentheses.

4 Additional illustrations of the crystal structures of $Li_{0.5-\delta}CoPO_4$ (*Cmcm*) and $Li_{1-\gamma}CoPO_4$ (*Cmcm*)

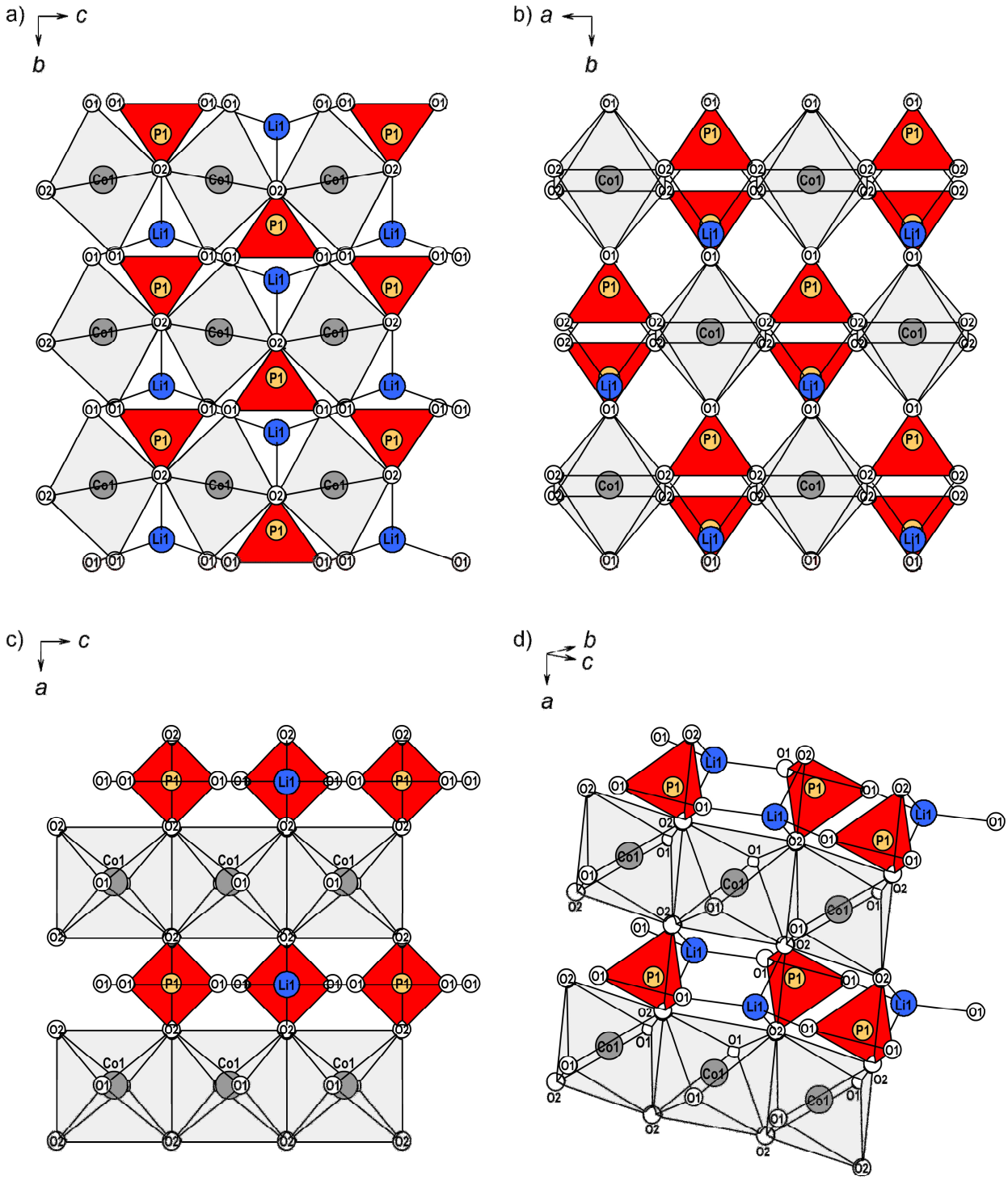

Figure S3 Detailed illustration of the crystal structures of *Cmcm*-type $Li_{0.5-\delta}CoPO_4$ and $Li_{1-\gamma}CoPO_4$ viewed along (a) [100], (b) [001], and (c) [010] (showing one layer of the composition $([CoO_6][LiO_4][PO_4])_\infty$). Li ions are drawn in blue, P atoms in orange, Co atoms in dark grey, and O atoms in white. $[CoO_6]$ octahedra are displayed in light grey, and $[PO_4]$ tetrahedra in red. The structure is built from $([CoO_6][LiO_4][PO_4])_\infty$ layers in the *ac* plane (c), which are stacked along *b* and connected *via* O1 atoms. In the layers, every $[CoO_6]$ octahedron shares two opposite O2–O2 edges with neighboring $[CoO_6]$ units, resulting in $[CoO_6]_\infty$ rows along [100], as well as two apical O2 atoms with two different $[PO_4]$ and $[LiO_4]$ tetrahedra (as demonstrated in d). The occupancies on the Li and Co sites are 39(2)% Li and 96.5(5)% Co for $Li_{0.5-\delta}CoPO_4$, and 94(2)% Li and 95.5(5)% Co for $Li_{1-\gamma}CoPO_4$.

5 Electrochemical stabilities (cycle life) of $Li_{0.5-\delta}CoPO_4$ (*Cmcm*) and $Li_{1-\gamma}CoPO_4$ (*Cmcm*)

Experimental details

The electrodes were prepared by mixing 80 wt% of the as-prepared lithium cobalt phosphate active material (*Cmcm*-type $Li_{0.5-\delta}CoPO_4$ or $Li_{1-\gamma}CoPO_4$), 10 wt% carbon (Super C65, Timcal), and 10 wt% polyvinylidene difluoride (PVDF, Solef, Solvay) binder in an agate mortar using *N*-methyl pyrrolidone (NMP) as solvent. The slurries were spread onto C-coated aluminum current collectors (Coveris Advanced Coatings) using a doctor-blade coater and then dried at 120 °C for 5 h in a vacuum oven (Thermo Scientific). The electrode sheets were calendered (International Rolling Mills device), and circular electrodes (diameter: 14.3 mm, average loading: ~4 mg) punched out. The electrochemical performance was tested using CR2032 coin cells with Li foil as anode (0.75 mm, Alfa Aesar, 99.9%, metals basis), a microporous monolayer PP membrane separator (Celgard 2400, 25 µm) and 1 M $LiPF_6$ in an ethylene carbonate (EC)/diethyl carbonate (DEC) mixture (1:1, *v*:*v*, Daikin) as electrolyte. The cells were assembled in an Ar-filled glove-box (VAC, < 0.1 ppm H_2O, < 0.1 ppm O_2). Charge–discharge cycling of two cells per material was carried out galvanostatically between 3.0 V and 5.2 V using a VMP3 multi-channel potentiostat/galvanostat (BioLogic) at 0.1 C, 0.2 C, 0.5 C, and 1 C for three cycles each in order to test the C rate capability, followed by 20 cycles at 0.1 C to evaluate the cycle life. Current densities and specific capacities were calculated using the weight of active material on the electrode. Note that the testing conditions, which were optimized for olivine-type $LiCoPO_4$ (*Pnma*), were not modified to improve the performance of the *Cmcm*-type materials.

Results and discussion

Since olivine-type $LiCoPO_4$ (*Pnma*) exhibits two two-phase redox reaction steps ($LiCoPO_4/Li_{2/3}CoPO_4$ and $Li_{2/3}CoPO_4/CoPO_4$)[4, 5] upon Li insertion–extraction, we assessed the electrochemical properties of both *Cmcm*-type materials, $Li_{0.5-\delta}CoPO_4$ and $Li_{1-\gamma}CoPO_4$, in order to elucidate whether the Li-deficient phase $Li_{0.5-\delta}CoPO_4$ represents an intermediate upon cycling of $Li_{1-\gamma}CoPO_4$ (*Cmcm*). The rate capabilities and coulombic efficiencies were investigated at 0.1 C, 0.2 C, 0.5 C, 1 C, and 2 C for three cycles each (Fig. S4a, inset), followed by 20 cycles at 0.1 C (Fig. S4b). The galvanostatic curves of the first cycle at 0.1 C (Fig. S4a) of both materials are similar despite the different Li contents and Co oxidation states and reveal that no plateau region is reached, which would be expected around ~4.3 V.[6] (Note that the corresponding curves at rates ≥ 0.2 C are not displayed as the capacities were extremely low). A discharge capacity of ~2.5 $mAh \cdot g^{-1}$ is obtained for both materials whereas the capacities upon first charge were 17 $mAh \cdot g^{-1}$ and 18 $mAh \cdot g^{-1}$, respectively. The large irreversible capacities are consistent with the high coulombic inefficiencies of about 85%, which indicate that irreversible reactions occur. The capacities are decreased upon further cycling. On basis of the comparably low capacities and the lack of a plateau region, it cannot be deduced whether $Li_{0.5-\delta}CoPO_4$ (*Cmcm*) represents an intermediate phase upon the delithiation of $Li_{1-\gamma}CoPO_4$ (*Cmcm*). The capacities and coulombic inefficiencies are most likely the result of the oxidation of cell components such as the conductive carbon and/or electrolyte decomposition at the high voltage used.[4, 7] Furthermore, the poor performance, which is in agreement with previous results on $LiCoPO_4$ (*Cmcm*)[6] is related to the intrinsically low Li-ion conductivities due to the lack of suitable Li migration pathways in the structure, as discussed in the main article. Therefore, future efforts should focus on optimizing the testing conditions (*e.g.* by the development of electrolyte suitable for the potential window) as well as the material (*e.g.* by carbon coating) in order to improve the performance and/or investigate the mechanisms which are responsible for the poor performance. The possibility of structural changes upon cycling might also be of special interest since the material is metastable (*cf.* thermal analysis section in the main article).

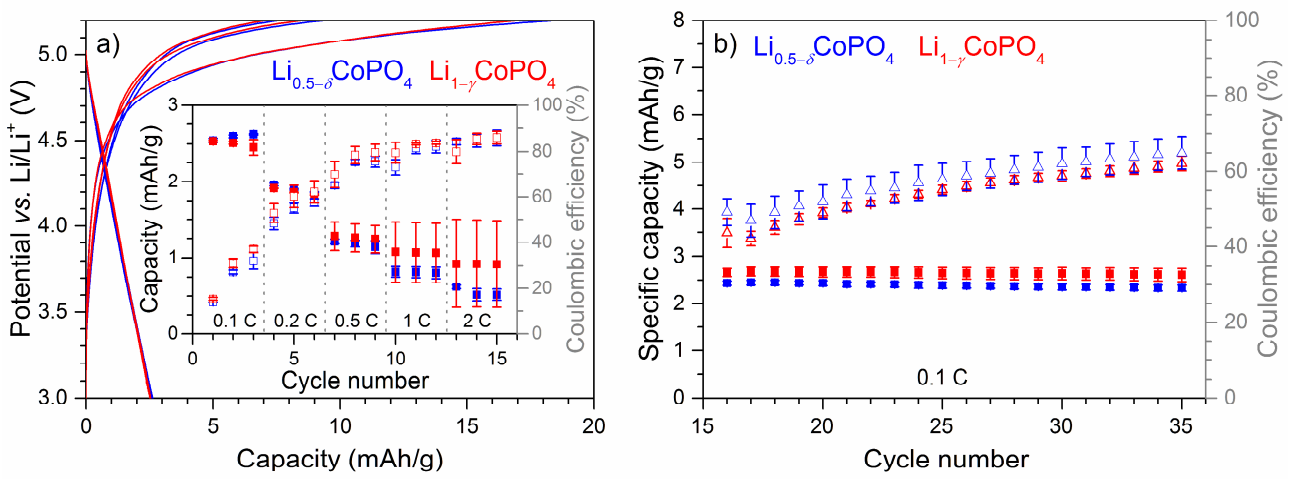

Figure S4 (a) Charge–discharge curves of $Li_{0.5-\delta}CoPO_4$ (*Cmcm*, blue), and $Li_{1-\gamma}CoPO_4$ (*Cmcm*, red) for the first three cycles at 0.1 C (the curves for rates ≥ 0.2 C are not shown as the capacities were very low). Inset: Specific discharge capacities (■) and coulombic efficiencies (□) vs. cycle number of both materials for the first 15 cycles at various C rates (capacities and error bars are derived from the values of two cells). (b) Specific discharge capacities (■) and respective coulombic efficiencies (Δ) (both average values from two cells) *vs.* cycle number of $Li_{0.5-\delta}CoPO_4$ (*Cmcm*, blue) and $Li_{1-\gamma}CoPO_4$ (*Cmcm*, red) for 20 cycles at 0.1 C after the first 15 cycles of C rate testing (a). The error bars represent the standard deviations from two cells. Conditions: 3.0–5.2 V, 1 M $LiPF_6$ in EC:DEC (1:1, v:v) at 25 °C.

6 Scanning electron microscopy (SEM) and energy-dispersive X-ray spectroscopy (EDS) of $Li_{0.5-\delta}CoPO_4$ (*Cmcm*) and $Li_{1-\gamma}CoPO_4$ (*Cmcm*)

Experimental details

A JEOL JSM-7500F high-resolution SEM using an accelerating voltage of 1 kV, a working distance of 8 mm, and a LEI (lower secondary electron image) detector was used to investigate the morphology of the material. Semi-quantitative EDS analysis was performed at an acceleration voltage of 15 kV and a probe current of 20 µA (Noran system S1X system, Thermo Electron Corporation, model 6714A01SUS-SN). The powder samples were prepared on conductive carbon tape which was attached to an aluminum stub.

Results and discussion

High-resolution SEM images (Fig. S5) reveal that both powders contain agglomerates with a dumbbell-like morphology. While the nanosheet-like primary particles of both materials are comparable in size and shape (length: ~50–100 nm, thickness: < 10 nm; Fig. S5b,e), the dumbbells of $Li_{0.5-\square}CoPO_4$ are about 3–4 times larger than the ones observed in $LiCoPO_4$ (~4 µm × 6 µm *vs.* ~1 µm × 2 µm; Fig. S5a,d). The different dimensions of the agglomerates are most likely related to the different precursor concentrations in the TTEG solvent. As for the production of *Cmcm*-type $LiCoPO_4$, a higher portion of lithium acetate was used (while the amounts of cobalt acetate and phosphoric acid remained unaltered), a higher degree of supersaturation was reached in the viscous solvent. Consequently, nucleation was favored over crystal growth processes under these conditions, producing smaller particles. Because no additives or organic templates are required to obtain these complex morphologies, it can be inferred that TTEG exhibits a soft template effect, which allows to direct the growth and self-assembly of hierarchical structures with preferred orientations.[8] EDS analysis delivers a composition of 37(3) wt% Co, 20.5(8) wt% P, and 43(2) wt% O for $Li_{0.5-\delta}CoPO_4$ (Fig. S5c), and 36(1) wt% Co, 20.7(3) wt% P, and 43.4(6) wt% O for $Li_{1-\gamma}CoPO_4$ (Fig. S5f), corresponding to Co:P:O molar ratios of 0.94(8):1.00(4):4.0(2) and 0.91(3):1.00(1):4.06(6), respectively. The deficit in Co found for both samples is in line with the results of the elemental analysis (*cf.* Table 2 in the main article).

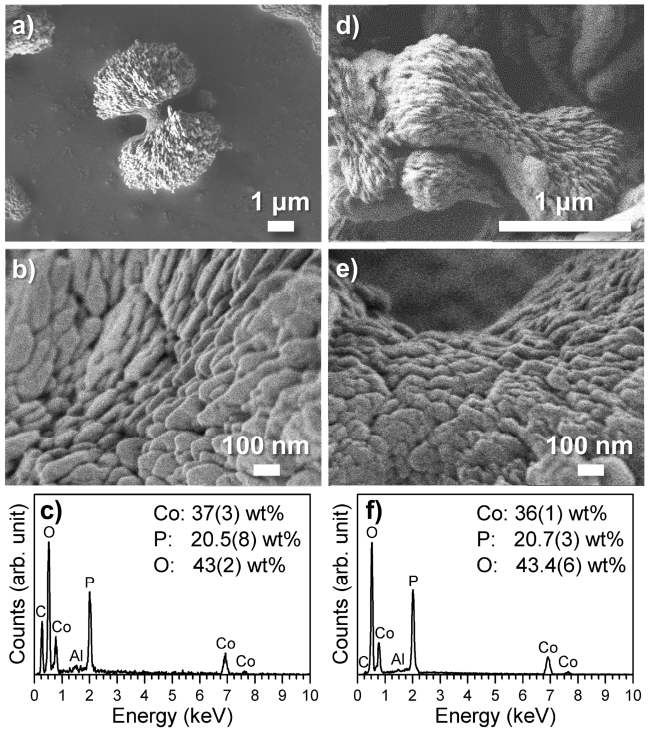

Figure S5 SEM images and corresponding EDS spectra of (a,b,c) $Li_{0.5-\delta}CoPO_4$ (*Cmcm*), and (d,e,f) $Li_{1-\gamma}CoPO_4$ (*Cmcm*). The C and Al signals observed in the EDS spectra (c,f) arise from the carbon tape and the aluminum sample holder used for the measurements.

7 Full infrared spectra of $Li_{0.5-\delta}CoPO_4$ (*Cmcm*) and $Li_{1-\gamma}CoPO_4$ (*Cmcm*)

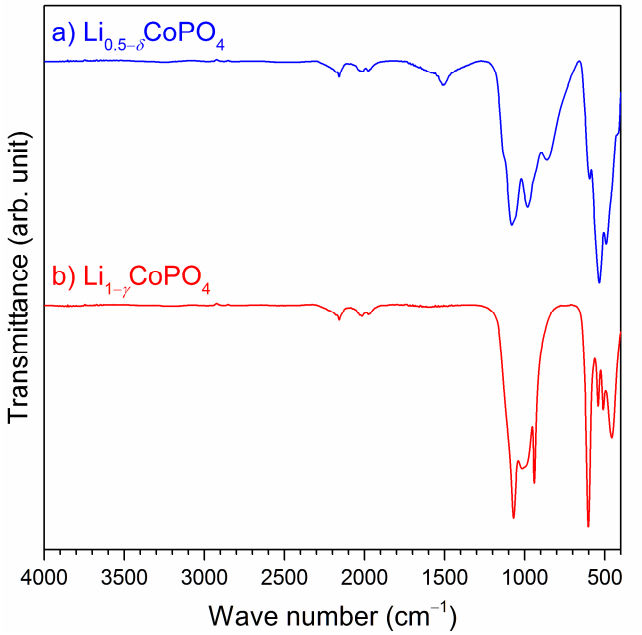

Figure S6 Comparison of the full FTIR spectra of (a) $Li_{0.5-\delta}CoPO_4$ (*Cmcm*, blue), and (b) $Li_{1-\gamma}CoPO_4$ (*Cmcm*, red, data reproduced from reference [1]). The samples do not contain any detectable amounts of water or other impurities. The absorption bands around 2000–2200 cm^{-1} are because of the diamond ATR setup.

8 Additional magnetic measurements of $Li_{0.5-\delta}CoPO_4$ (*Cmcm*) and $Li_{1-\gamma}CoPO_4$ (*Cmcm*)

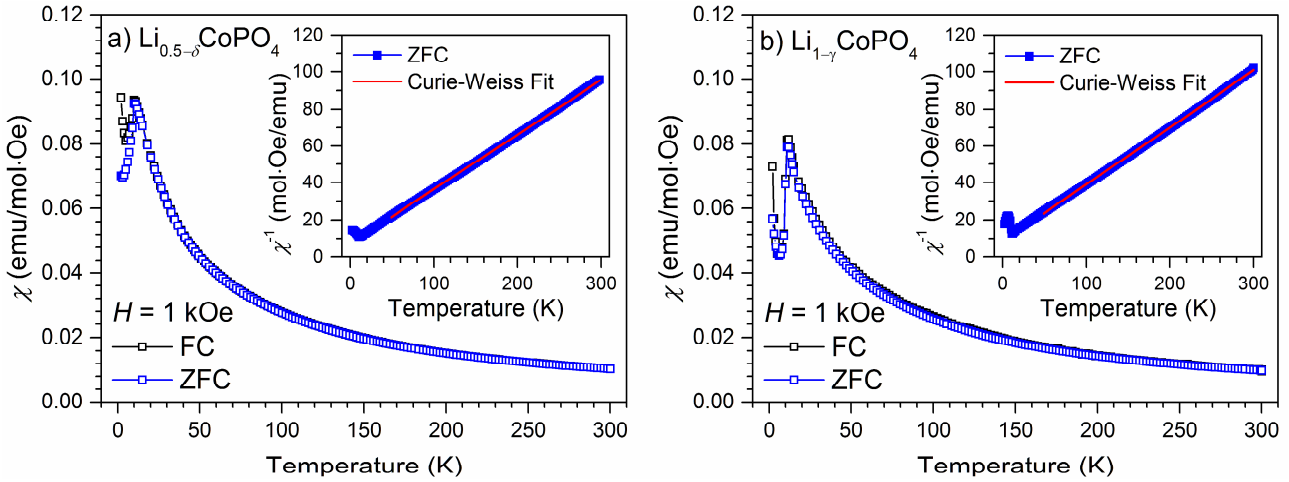

Figure S7 Magnetic susceptibility as a function of the temperature of (a) $Li_{0.5-\delta}CoPO_4$ (*Cmcm*), and (b) $Li_{1-\gamma}CoPO_4$ (*Cmcm*) at zero-field-cooled (ZFC) and field-cooled (FC) conditions under a constant applied field of 1 kOe. The insets show the inverse magnetic susceptibility and the Curie–Weiss fitting from $T = 50$ K to 300 K under ZFC conditions. The temperature dependence of the magnetic susceptibility indicates an antiferromagnetic order below the Néel-temperatures of $T_N = 10.5$ K and 11 K for $Li_{0.5-\delta}CoPO_4$ (*Cmcm*) and $Li_{1-\gamma}CoPO_4$ (*Cmcm*), respectively. In the high-temperature region, the inverse magnetic susceptibility is well described by the Curie–Weiss law. The fit to the data delivers effective magnetic moments of $\mu_{eff} = (5.20 \pm 0.02)\ \mu_B$ for $Li_{0.5-\delta}CoPO_4$ and $(5.08 \pm 0.02)\ \mu_B$ for $Li_{1-\gamma}CoPO_4$, respectively.

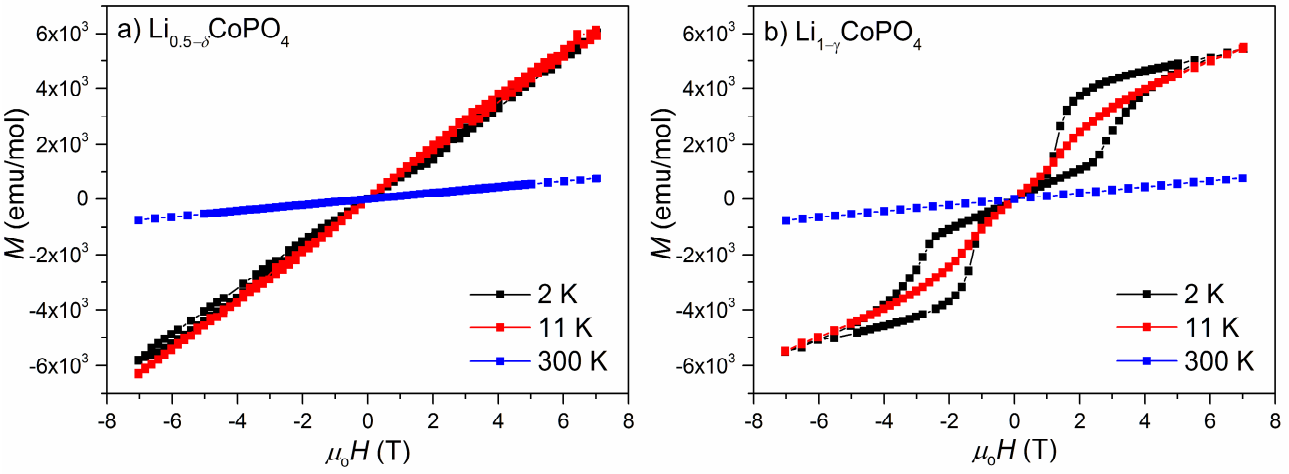

Figure S8 Magnetization as a function of the applied magnetic field between 7 and −7 T of (a) $Li_{0.5-\delta}CoPO_4$ (*Cmcm*), and (b) $Li_{1-\gamma}CoPO_4$ (*Cmcm*) recorded at temperatures of 2 K, 11 K, and 300 K, respectively. In contrast to the $Li_{1-\gamma}CoPO_4$ compound, no spin-flip transitions indicated by the double-hysteresis loop could be observed at low temperature in the Li-deficient $Li_{0.5-\delta}CoPO_4$ phase. Furthermore, no indication of a weak ferromagnetic component due to the mixed-valence state of the Co ions could be found in the magnetic hysteresis loops.

9 Rietveld refinement of the sample obtained after the TGA/DSC measurement of $Li_{0.5-\delta}CoPO_4$ (*Cmcm*) under synthetic air

Table S7 Crystallographic details and phase fractions of the phases observed in the X-ray powder diffraction pattern (T = 298 K) of the post-TGA/DSC (temperature range: 30–900 °C, atmosphere: synthetic air; *cf.* Fig. 6) sample of $Li_{0.5-\delta}CoPO_4$ (*Cmcm*) [a]

Phase	$LiCoPO_4$	α-$Co_2P_2O_7$
Space group	*Pnma*	$P2_1/c$
Phase fraction (wt%)	44.9(6)	55.1(6)
Z	4	4
a (Å)	10.2073(5)	7.0065(4)
b (Å)	5.9227(3)	8.3631(5)
c (Å)	4.7008(3)	9.0096(5)
α (°)	90	90
β (°)	90	113.648(3)
γ (°)	90	90
V (Å^3)	284.18(3)	483.60(5)
F(000)	560	
ρ (calcd.) (g·cm^{-3})	3.759(1)	4.008(1)
R_p	0.0411	
R_{wp}	0.0595	
R_{exp}	0.0328	
R_F	0.0374	0.0367
R_B	0.0565	0.0565
χ^2	1.82	
Data/restraints/parameter	3808/0/118	

[a] The estimated standard deviations were calculated by the Berar's procedure and are indicated in parentheses.

Table S8 Fractional atomic coordinates and isotropic thermal displacement parameters of $LiCoPO_4$ (*Pnma*, *Z* = 4) as refined from X-ray powder diffraction data (*T* = 298 K) of the post-TGA/DSC (temperature range: 30–900 °C, atmosphere: synthetic air) sample of $Li_{0.5-\delta}CoPO_4$ (*Cmcm*) [a]

Atom	Wyckoff position	Occupancy	*x*/a	*y*/b	*z*/c	U_{iso} (Å^2)
Li1	4*a*	1	0	0	0	0.0139 [b]
Co1	4*c*	1	0.2214(3)	¼	0.5212(9)	0.0109(15)
P1	4*c*	1	0.4046(8)	¼	0.0808(16)	0.013(2)
O1	4*c*	1	0.4052(19)	¼	0.761(3)	0.007(3)
O2	4*c*	1	0.048(2)	¼	0.298(3)	0.008(2)
O3	8*d*	1	0.3345(15)	0.047(2)	0.218(2)	0.007(2)

[a] The estimated standard deviations were calculated by the Berar's procedure and are indicated in parentheses. [b] Li positions and thermal displacement parameters have been fixed as they cannot be deduced by means of X-ray diffraction due to the low atomic scattering factor of Li.

Table S9 Selected interatomic distances of $LiCoPO_4$ (*Pnma*, *Z* = 4) as refined from X-ray powder diffraction data (*T* = 298 K) of the post-TGA/DSC (temperature range: 30–900 °C, atmosphere: synthetic air) sample of $Li_{0.5-\delta}CoPO_4$ (*Cmcm*) [a]

Atom pair			*d* (Å)
Li1	O1	×2	2.152(12)
	O2	×2	2.095(11)
	O3	×2	2.165(14)
	Li1–O average		2.137
Co1	O1	×1	2.189(19)
	O2	×1	2.06(2)
	O3	×2	2.068(12)
	O3	×2	2.192(13)
	Co1–O average		2.128
P1	O1	×1	1.504(16)
	O2	×1	1.57(2)
	O3	×2	1.541(14)
	P1–O average		1.539

[a] The estimated standard deviations were calculated by the Berar's procedure and are indicated in parentheses.

Table S10 Fractional atomic coordinates and isotropic thermal displacement parameters of α-$Co_2P_2O_7$ ($P2_1/c$, $Z = 4$) as refined from X-ray powder diffraction data ($T = 298$ K) of post-TGA/DSC (temperature range: 30–900 °C, atmosphere: synthetic air) sample of $Li_{0.5-\delta}CoPO_4$ (*Cmcm*) [a]

Atom	Wyckoff position	Occupancy	*x*/a	*y*/b	*z*/c	U_{iso} (Å^2)
Co1	4*e*	1	0.2329(16)	0.9293(9)	0.1088(13)	0.012(2)
Co2	4*e*	1	0.7001(12)	0.4421(11)	0.8248(9)	0.014(3)
P1	4*e*	1	0.942(3)	0.7656(19)	0.758(2)	0.011(5)
P2	4*e*	1	0.534(3)	0.7744(19)	0.468(2)	0.010(5)
O1	4*e*	1	0.751(7)	0.830(3)	0.605(5)	0.010(4)
O2	4*e*	1	0.378(6)	0.766(4)	0.549(4)	0.006(4)
O3	4*e*	1	1.120(5)	0.755(3)	0.705(4)	0.005(5)
O4	4*e*	1	0.979(7)	0.906(5)	0.880(4)	0.009(4)
O5	4*e*	1	0.886(5)	0.607(5)	0.816(4)	0.008(5)
O6	4*e*	1	0.486(5)	0.908(4)	0.340(4)	0.007(4)
O7	4*e*	1	0.555(6)	0.615(4)	0.397(4)	0.006(5)

[a] The estimated standard deviations were calculated by the Berar's procedure and are indicated in parentheses.

Table S11 Selected interatomic distances of α-$Co_2P_2O_7$ ($P2_1/c$, $Z = 4$) as refined from X-ray powder diffraction data ($T = 298$ K) of the post-TGA/DSC (temperature range: 30–900 °C, atmosphere: synthetic air) sample of $Li_{0.5-\delta}CoPO_4$ (*Cmcm*) [a]

Atom pair			***d*** **(Å)**
Co1	O2	×1	2.11(4)
	O3	×1	2.08(4)
	O4	×1	2.06(5)
	O4	×1	2.13(3)
	O6	×1	2.14(3)
	O7	×1	2.17(4)
	Co1–O average		2.12
Co2	O2	×1	2.06(4)
	O3	×1	2.09(4)
	O5	×1	1.92(4)
	O6	×1	2.00(4)
	O7	×1	2.13(3)
	Co2–O average		2.04
P1	O1	×1	1.58(4)
	O3	×1	1.51(5)
	O4	×1	1.55(5)
	O5	×1	1.53(4)
	P1–O average		1.54
P2	O1	×1	1.59(4)
	O2	×1	1.54(5)
	O6	×1	1.54(4)
	O7	×1	1.51(4)
	P2–O average		1.55

[a] The estimated standard deviations were calculated by the Berar's procedure and are indicated in parentheses.

10 Thermal stability of $Li_{0.5-\delta}CoPO_4$ (*Cmcm*) under Ar

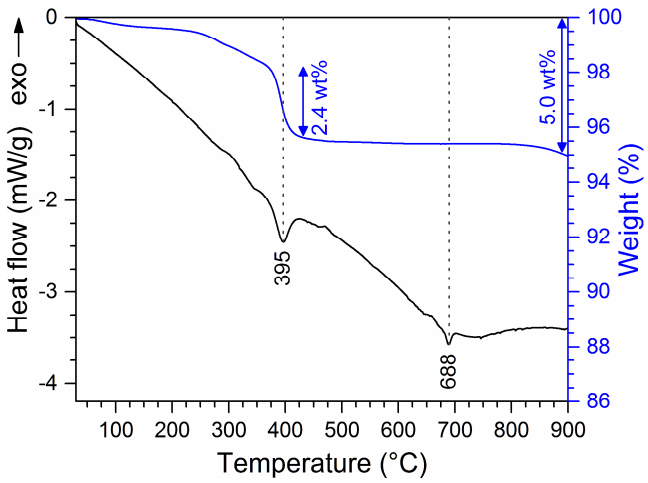

Figure S9 DSC (black) and TGA (blue) curves of $Li_{0.5-\delta}CoPO_4$ (*Cmcm*) measured in a temperature range of 30–900 °C (heating rate: 10 °C·min^{-1}) under Ar. Two endothermic signals are observed in the DSC curve at 395 °C (accompanied by a weight loss step of ~2.4 wt%) and 688 °C, respectively. The data are in good agreement with the TGA/DSC measurement performed under synthetic air (*cf.* Fig. 6 in the main article).

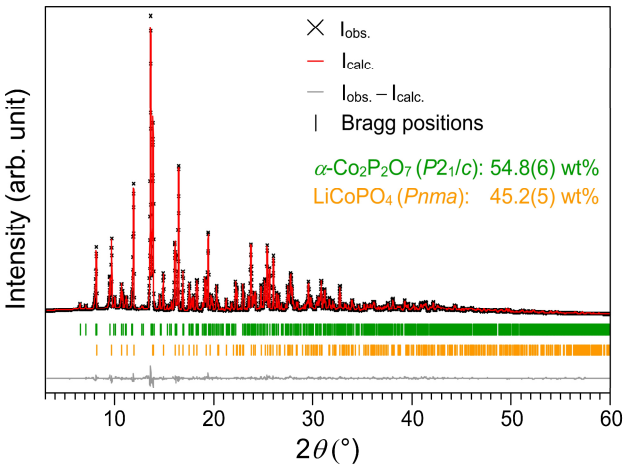

Figure S10 Rietveld fit of the X-ray powder diffraction data (transmission geometry, Mo $K_{\alpha1}$ radiation) of the dark violet material obtained after the TGA/DSC measurement of $Li_{0.5-\delta}CoPO_4$ (*Cmcm*) under Ar (T = 30–900 °C, heating rate: 10 °C·min^{-1}; *cf.* Fig. S9). Similar to the material obtained from the TGA/DSC measurement under synthetic air (*cf.* Fig. 6 in the main article), a mixture of olivine-type $LiCoPO_4$ (*Pnma*) and α-$Co_2P_2O_7$ ($P2_1/c$) was formed upon heating.

Table S12 Crystallographic details and phase fractions of the phases observed in the X-ray powder diffraction pattern (T = 298 K) of the post-TGA/DSC (temperature range: 30–900 °C, atmosphere: Ar; *cf.* Fig. S9) sample of $Li_{0.5-\delta}CoPO_4$ (*Cmcm*) [a]

Phase	**$LiCoPO_4$**	**α-$Co_2P_2O_7$**
Space group	***Pnma***	***$P2_1/c$***
Phase fraction (wt%)	**45.2(5)**	**54.8(6)**
Z	4	4
a (Å)	10.2108(5)	7.0089(4)
b (Å)	5.9247(3)	8.3659(5)
c (Å)	4.7025(2)	9.0127(5)
α (°)	90	90
β (°)	90	113.647(3)
γ (°)	90	90
V (Å^3)	284.48(3)	484.10(5)
F(000)	560	
ρ (calcd.) (g·cm^{-3})	3.756(1)	4.004(1)
R_p	0.0414	
R_{wp}	0.0599	
R_{exp}	0.0330	
R_F	0.0362	0.0347
R_B	0.0557	0.0534
χ^2	1.82	
Data/restraints/parameter	3803/0/118	

[a] The estimated standard deviations were calculated by the Berar's procedure and are indicated in parentheses.

Table S13 Fractional atomic coordinates and isotropic thermal displacement parameters of $LiCoPO_4$ (*Pnma*, *Z* = 4) as refined from X-ray powder diffraction data (*T* = 298 K) of the post-TGA/DSC (temperature range: 30–900 °C, atmosphere: Ar) sample of $Li_{0.5-\delta}CoPO_4$ (*Cmcm*) [a]

Atom	Wyckoff position	Occupancy	*x*/a	*y*/b	*z*/c	U_{iso} (Å^2)
Li1	4*a*	1	0	0	0	0.0139 [b]
Co1	4*c*	1	0.2215(3)	¼	0.5209(9)	0.0113(15)
P1	4*c*	1	0.4048(8)	¼	0.0806(15)	0.012(2)
O1	4*c*	1	0.4046(19)	¼	0.760(3)	0.005(3)
O2	4*c*	1	0.048(2)	¼	0.297(3)	0.008(2)
O3	8*d*	1	0.3344(15)	0.046(2)	0.217(2)	0.006(2)

[a] The estimated standard deviations were calculated by the Berar's procedure and are indicated in parentheses. [b] The Li position and thermal displacement parameter have been fixed as they cannot be deduced by means of X-ray diffraction due to the low atomic scattering factor of Li.

Table S14 Selected interatomic distances of $LiCoPO_4$ (*Pnma*, *Z* = 4) as refined from X-ray powder diffraction data (*T* = 298 K) of the post-TGA/DSC (temperature range: 30–900 °C, atmosphere: Ar) sample of $Li_{0.5-\delta}CoPO_4$ (*Cmcm*) [a]

Atom pair			*d* (Å)
Li1	O1	×2	2.154(12)
	O2	×2	2.097(11)
	O3	×2	2.166(13)
	Li1–O average		2.14
Co1	O1	×1	2.182(18)
	O2	×1	2.06(2)
	O3	×2	2.067(12)
	O3	×2	2.194(12)
	Co1–O average		2.13
P1	O1	×1	1.507(16)
	O2	×1	1.57(2)
	O3	×2	1.545(13)
	P1–O average		1.54

[a] The estimated standard deviations were calculated by the Berar's procedure and are indicated in parentheses.

Table S15 Fractional atomic coordinates and isotropic thermal displacement parameters of α-$Co_2P_2O_7$ ($P2_1/c$, $Z = 4$) as refined from X-ray powder diffraction data ($T = 298$ K) of the post-TGA/DSC (temperature range: 30–900 °C, atmosphere: Ar) sample of $Li_{0.5-\delta}CoPO_4$ (*Cmcm*) [a]

Atom	Wyckoff position	Occupancy	*x*/a	*y*/b	*z*/c	U_{iso} (Å^2)
Co1	4*e*	1	0.2334(16)	0.9295(8)	0.1091(13)	0.010(2)
Co2	4*e*	1	0.6998(12)	0.4418(10)	0.8248(9)	0.013(3)
P1	4*e*	1	0.943(3)	0.7666(19)	0.759(2)	0.012(5)
P2	4*e*	1	0.536(3)	0.7742(19)	0.469(2)	0.010(5)
O1	4*e*	1	0.750(7)	0.831(3)	0.606(5)	0.013(5)
O2	4*e*	1	0.377(5)	0.767(4)	0.549(4)	0.009(4)
O3	4*e*	1	1.119(5)	0.754(3)	0.704(4)	0.011(3)
O4	4*e*	1	0.980(7)	0.907(5)	0.880(4)	0.010(3)
O5	4*e*	1	0.884(5)	0.607(5)	0.815(4)	0.009(3)
O6	4*e*	1	0.487(5)	0.907(4)	0.340(3)	0.005(2)
O7	4*e*	1	0.555(5)	0.616(4)	0.398(3)	0.006(2)

[a] The estimated standard deviations were calculated by the Berar's procedure and are indicated in parentheses.

Table S16 Selected interatomic distances of α-$Co_2P_2O_7$ ($P2_1/c$, $Z = 4$) as refined from X-ray powder diffraction data (T = 298 K) of the post-TGA/DSC (temperature range: 30–900 °C, atmosphere: Ar) sample of $Li_{0.5-\delta}CoPO_4$ (*Cmcm*) [a]

Atom pair			*d* (Å)
Co1	O2	×1	2.11(4)
	O3	×1	2.07(4)
	O4	×1	2.06(5)
	O4	×1	2.12(3)
	O6	×1	2.14(3)
	O7	×1	2.17(4)
	Co1–O average		2.11
Co2	O2	×1	2.05(4)
	O3	×1	2.10(3)
	O5	×1	1.92(4)
	O6	×1	2.01(4)
	O7	×1	2.14(3)
	Co2–O average		2.04
P1	O1	×1	1.59(4)
	O3	×1	1.51(5)
	O4	×1	1.55(5)
	O5	×1	1.54(4)
	P1–O average		1.55
P2	O1	×1	1.58(4)
	O2	×1	1.55(5)
	O6	×1	1.54(3)
	O7	×1	1.50(4)
	P2–O average		1.54

[a] The estimated standard deviations were calculated by the Berar's procedure and are indicated in parentheses.

11 Rietveld refinements of the *in situ* X-ray powder diffraction patterns upon heating of $Li_{0.5-\delta}CoPO_4$ (*Cmcm*) under air in the temperature range of 30–700 °C

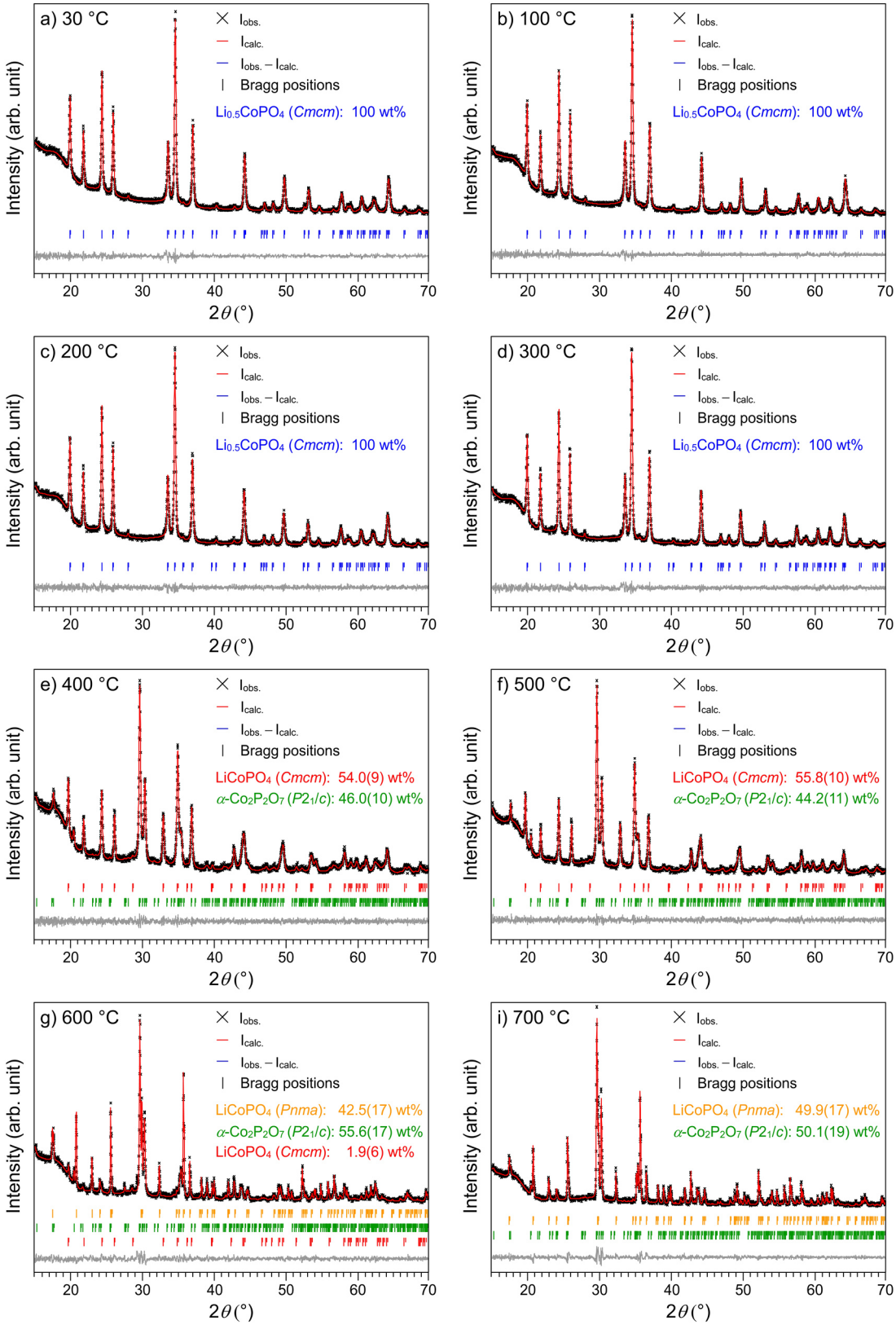

Figure S11 Rietveld fits of the *in situ* X-ray powder diffraction patterns (Bragg-Brentano geometry, Cu K_α radiation) of $Li_{0.5-\delta}CoPO_4$ (*Cmcm*; with $\delta = 0$) between 30 °C and 700 °C under air. The data at 800 °C, 900 °C, and after cooling to 25 °C are not shown because mainly reflections caused by the corundum sample holder were observed, which did not allow for a refinement of the phase fractions (*cf.* Fig. S12). Note that the Bragg reflections indicate the $K_{\alpha1}$ and $K_{\alpha2}$ peaks.

Table S17 Crystallographic details and phase fractions of the phases observed in the *in situ* X-ray powder diffraction patterns of $Li_{0.5-\delta}CoPO_4$ (*Cmcm*) between 30 °C and 700 °C under air [a]

Temperature	**a) 30 °C**	**b) 100 °C**	**c) 200 °C**	**d) 300 °C**	**e) 400 °C**		**f) 500 °C**		**g) 600 °C** [d]		**h) 700 °C**	
Phase	$Li_{0.5}CoPO_4$ [b]	$Li_{0.5}CoPO_4$ [b]	$Li_{0.5}CoPO_4$ [b]	$Li_{0.5}CoPO_4$ [b]	$LiCoPO_4$ [c]	α-$Co_2P_2O_7$	$LiCoPO_4$ [c]	α-$Co_2P_2O_7$	$LiCoPO_4$	α-$Co_2P_2O_7$	$LiCoPO_4$	α-$Co_2P_2O_7$
Space group	*Cmcm*	*Cmcm*	*Cmcm*	*Cmcm*	*Cmcm*	$P2_1/c$	*Cmcm*	$P2_1/c$	*Pnma*	$P2_1/c$	*Pnma*	$P2_1/c$
Phase fraction (wt%)	**100**	**100**	**100**	**100**	**54.0(9)**	**46.0(10)**	**55.8(10)**	**44.2(11)**	**42.5(17)**	**55.6(17)**	**49.9(17)**	**50.1(19)**
Z	4	4	4	4	4	4	4	4	4	4	4	4
a (Å)	5.3378(4)	5.3416(3)	5.3496(4)	5.3505(4)	5.4612(6)	7.0109(13)	5.4695(6)	7.0163(12)	10.2763(8)	7.0239(16)	10.2952(10)	7.0238(9)
b (Å)	8.1746(5)	8.1812(5)	8.1956(5)	8.2057(6)	8.2012(8)	8.3650(16)	8.2142(9)	8.3706(15)	6.0031(5)	8.3702(18)	6.0191(5)	8.3836(10)
c (Å)	6.3694(4)	6.3751(3)	6.3842(4)	6.4050(4)	6.2569(6)	9.0391(16)	6.2645(6)	9.0462(16)	4.7528(5)	9.0543(19)	4.7624(5)	9.0593(12)
α (°)	90	90	90	90	90	90	90	90	90	90	90	90
β (°)	90	90	90	90	90	114.218(8)	90	114.137(8)	90	114.067(12)	90	113.997(7)
γ (°)	90	90	90	90	90	90	90	90	90	90	90	90
V (Å^3)	277.93(3)	278.60(3)	279.90(3)	281.21(3)	280.24(5)	483.45(16)	281.44(5)	484.84(15)	293.19(5)	486.04(19)	295.11(5)	487.35(11)
F(000)	302	302	302	302	560		560		308		560	
ρ (calcd.) (g·cm^{-3})	3.761(1)	3.752(1)	3.735(1)	3.717(1)	3.812(1)	4.009(1)	3.796(1)	3.998(1)	3.644(1)	3.988(1)	3.620(1)	3.977(1)
R_p	0.0326	0.0333	0.0340	0.0357	0.0342		0.0349		0.0469		0.0525	
R_{wp}	0.0425	0.0431	0.0445	0.0462	0.0437		0.0458		0.0618		0.0709	
R_{exp}	0.0377	0.0383	0.0388	0.0392	0.0393		0.0396		0.0396		0.0407	
R_F	0.0187	0.0164	0.0186	0.0220	0.0155	0.0251	0.0207	0.0250	0.0371	0.0489	0.0600	0.0406
R_B	0.0456	0.0456	0.0456	0.0456	0.0264	0.0325	0.0320	0.0380	0.0614	0.0716	0.1013	0.0550
χ^2	1.13	1.12	1.15	1.18	1.11		1.16		1.56		1.74	
Data/restraints/ parameter	3291/0/52	3291/0/52	3291/0/52	3291/0/52	3291/0/104		3291/0/104		3291/0/111		3291/0/111	

[a] The estimated standard deviations were calculated by the Berar's procedure and are indicated in parentheses. [b] $Li_{0.5-\delta}CoPO_4$ with $\delta = 0$ for simplicity. [c] $Li_{1-\gamma}CoPO_4$ with $\gamma = 0$ for simplicity.
[d] The cell parameters of the third phase $LiCoPO_4$ (*Cmcm*) were not refined as the phase fraction accounted for only 1.9(6) wt% (*cf.* Fig. S11).

Table S18 Fractional atomic coordinates and isotropic thermal displacement parameters of $Li_{0.5}CoPO_4$ ($Li_{0.5-\delta}CoPO_4$ with $\delta = 0$, *Cmcm*, $Z = 4$) as refined from temperature-dependent *in situ* X-ray powder diffraction data at 30 °C, 100 °C, 200 °C, and 300 °C [a]

Temperature	Atom	Wyck. position	Occupancy	*x*/a	*y*/b	*z*/c	U_{iso} (Å^2)
a) 30 °C	Li1	4*c*	0.5 [b]	0	0.675 [c]	¼	0.019 [c]
	Co1	4*a*	1	0	0	0	0.0136(17)
	P1	4*c*	1	0	0.3578(8)	¼	0.0053(15)
	O1	8*f*	1	0	0.2540(6)	0.0555(12)	0.0048(13)
	O2	8*g*	1	0.2427(10)	0.4631(8)	¼	0.0052(13)
b) 100 °C	Li1	4*c*	0.5 [b]	0	0.675 [c]	¼	0.019 [c]
	Co1	4*a*	1	0	0	0	0.0136(15)
	P1	4*c*	1	0	0.3587(7)	¼	0.0040(18)
	O1	8*f*	1	0	0.2544(5)	0.0580(11)	0.0046(12)
	O2	8*g*	1	0.2416(9)	0.4625(7)	¼	0.0048(12)
c) 200 °C	Li1	4*c*	0.5 [b]	0	0.675 [c]	¼	0.019 [c]
	Co1	4*a*	1	0	0	0	0.0142(18)
	P1	4*c*	1	0	0.3582(8)	¼	0.0056(12)
	O1	8*f*	1	0	0.2539(6)	0.0575(12)	0.0053(13)
	O2	8*g*	1	0.2430(10)	0.4614(8)	¼	0.0055(13)
d) 300 °C	Li1	4*c*	0.5 [b]	0	0.675 [c]	¼	0.019 [c]
	Co1	4*a*	1	0	0	0	0.0149(20)
	P1	4*c*	1	0	0.3565(9)	¼	0.0058(12)
	O1	8*f*	1	0	0.2528(7)	0.0564(15)	0.0055(13)
	O2	8*g*	1	0.2447(12)	0.4637(9)	¼	0.0059(13)

[a] The estimated standard deviations were calculated by the Berar's procedure and are indicated in parentheses. [b] The Li occupancy factors were kept fixed at 50% ($\delta = 0$). [c] Li positions and thermal displacement parameters have been fixed as they cannot be deduced by means of X-ray diffraction due to the low atomic scattering factor of Li.

Table S19 Selected interatomic distances of $Li_{0.5}CoPO_4$ ($Li_{0.5-\delta}CoPO_4$ with $\delta = 0$, *Cmcm*, $Z = 4$) as refined from temperature-dependent *in situ* X-ray powder diffraction data at 30 °C, 100 °C, 200 °C, and 300 °C [a]

	Atom pair		*d* (Å)			
			a) 30 °C	**b) 100 °C**	**c) 200 °C**	**d) 300 °C**
Li1	O1	×2	2.031(8)	2.047(7)	2.048(8)	2.050(9)
	O2	×2	2.163(6)	2.165(5)	2.180(6)	2.172(7)
	Li1–O average		2.097	2.106	2.114	2.111
Co1	O1	×2	2.106(5)	2.114(4)	2.113(5)	2.106(6)
	O2	×4	2.124(4)	2.131(3)	2.130(4)	2.126(4)
	Co1–O average		2.118	2.125	2.124	2.119
P1	O1	×2	1.502(8)	1.492(7)	1.497(8)	1.504(9)
	O2	×2	1.555(7)	1.545(6)	1.551(7)	1.577(8)
	P1–O average		1.529	1.519	1.524	1.541

[a] The estimated standard deviations were calculated by the Berar's procedure and are indicated in parentheses.

Table S20 Fractional atomic coordinates and isotropic thermal displacement parameters of $LiCoPO_4$ ($Li_{1-\gamma}CoPO_4$ with $\gamma = 0$, *Cmcm*, $Z = 4$) as refined from temperature-dependent *in situ* X-ray powder diffraction data at 400 °C and 500 °C [a]

Temperature	Atom	Wyck. position	Occupancy	*x*/a	*y*/b	*z*/c	U_{iso} (Å^2)
a) 400 °C	Li1	4*c*	1 [b]	0	0.675 [c]	¼	0.019 [c]
	Co1	4*a*	1	0	0	0	0.015(5)
	P1	4*c*	1	0	0.3506(16)	¼	0.007(7)
	O1	8*f*	1	0	0.2517(11)	0.046(2)	0.008(6)
	O2	8*g*	1	0.2343(17)	0.4625(13)	¼	0.009(6)
b) 500 °C	Li1	4*c*	1 [b]	0	0.675 [c]	¼	0.019 [c]
	Co1	4*a*	1	0	0	0	0.017(4)
	P1	4*c*	1	0	0.3525(16)	¼	0.012(6)
	O1	8*f*	1	0	0.2522(11)	0.047(2)	0.014(6)
	O2	8*g*	1	0.239(2)	0.4675(13)	¼	0.013(6)

[a] The estimated standard deviations were calculated by the Berar's procedure and are indicated in parentheses. [b] The Li occupancy factors were kept fixed at 100% ($\gamma = 0$). [c] Li positions and thermal displacement parameters have been fixed as they cannot be deduced by means of X-ray diffraction due to the low atomic scattering factor of Li.

Table S21 Selected interatomic distances of $LiCoPO_4$ ($Li_{1-\gamma}CoPO_4$ with $\gamma = 0$, *Cmcm*, $Z = 4$) as refined from temperature-dependent *in situ* X-ray powder diffraction data at 400 °C and 500 °C [a]

Atom pair			*d* (Å)	
			a) 400 °C	**b) 500 °C**
Li1	O1	×2	1.947(15)	1.957(14)
	O2	×2	2.162(10)	2.147(11)
	Li1–O average		2.055	2.052
Co1	O1	×2	2.084(9)	2.093(9)
	O2	×4	2.156(6)	2.137(7)
	Co1–O average		2.132	2.122
P1	O1	×2	1.512(15)	1.513(15)
	O2	×2	1.574(12)	1.612(13)
	P1–O average		1.543	1.563

[a] The estimated standard deviations were calculated by the Berar's procedure and are indicated in parentheses.

Table S22 Fractional atomic coordinates and isotropic thermal displacement parameters of $LiCoPO_4$ (*Pnma*, *Z* = 4) as refined from temperature-dependent *in situ* X-ray powder diffraction data at 600 °C and 700 °C [a]

Temperature	Atom	Wyck. position	Occupancy	*x*/a	*y*/b	*z*/c	U_{iso} (Å^2)
a) 600 °C	Li1	4*a*	1	0	0	0	0.0139 [b]
	Co1	4*c*	1	0.2206(9)	¼	0.527(3)	0.015(7)
	P1	4*c*	1	0.4028(17)	¼	0.070(5)	0.010(9)
	O1	4*c*	1	0.407(4)	¼	0.756(8)	0.009(16)
	O2	4*c*	1	0.046(5)	¼	0.285(6)	0.008(14)
	O3	8*d*	1	0.343(3)	0.059(5)	0.225(5)	0.010(14)
b) 700 °C	Li1	4*a*	1	0	0	0	0.0139 [b]
	Co1	4*c*	1	0.2192(10)	¼	0.533(3)	0.016(8)
	P1	4*c*	1	0.401(2)	¼	0.083(6)	0.012(10)
	O1	4*c*	1	0.417(5)	¼	0.773(11)	0.012(12)
	O2	4*c*	1	0.050(4)	¼	0.263(6)	0.013(13)
	O3	8*d*	1	0.350(3)	0.057(6)	0.228(5)	0.014(14)

[a] The estimated standard deviations were calculated by the Berar's procedure and are indicated in parentheses. [b] The thermal displacement parameters of Li have been fixed as they cannot be deduced by means of X-ray diffraction due to the low atomic scattering factor of Li.

Table S23 Selected interatomic distances of $LiCoPO_4$ (*Pnma*, *Z* = 4) as refined from temperature-dependent *in situ* X-ray powder diffraction data at 600 °C and 700 °C [a]

Atom pair			*d* (Å)	
			a) 600 °C	**b) 700 °C**
Li1	O1	×2	2.16(3)	2.16(4)
	O2	×2	2.08(2)	2.03(2)
	O3	×2	2.11(3)	2.04(3)
	Li1–O average		2.12	2.08
Co1	O1	×1	2.20(4)	2.34(5)
	O2	×1	2.13(5)	2.16(4)
	O3	×2	2.18(3)	2.19(3)
	O3	×2	2.23(3)	2.29(3)
	Co1–O average		2.19	2.24
P1	O1	×1	1.49(5)	1.48(6)
	O2	×1	1.63(5)	1.70(5)
	O3	×2	1.49(3)	1.45(3)
	P1–O average		1.53	1.52

[a] The estimated standard deviations were calculated by the Berar's procedure and are indicated in parentheses.

Table S24 Fractional atomic coordinates and isotropic thermal displacement parameters of α-$Co_2P_2O_7$ ($P2_1/c$, $Z = 4$) as refined from temperature-dependent *in situ* X-ray powder diffraction data at 400–700 °C [a]

Temperature	Atom	Wyck. position	Occupancy	*x*/a	*y*/b	*z*/c	U_{iso} (Å^2)
a) 400 °C	Co1	4*e*	1	0.241(6)	0.947(4)	0.864(5)	0.016(12)
	Co2	4*e*	1	0.235(6)	0.563(4)	0.871(6)	0.019(12)
	P1	4*e*	1	0.435(7)	0.266(6)	0.763(5)	0.008(18)
	P2	4*e*	1	0.006(5)	0.239(6)	0.460(3)	0.007(13)
	O1	4*e*	1	0.234(14)	0.180(7)	0.589(9)	0.008(12)
	O2	4*e*	1	−0.115(11)	0.314(9)	0.567(10)	0.005(13)
	O3	4*e*	1	0.625(14)	0.252(13)	0.722(9)	0.006(13)
	O4	4*e*	1	0.497(14)	0.086(15)	0.911(13)	0.007(14)
	O5	4*e*	1	0.427(12)	0.415(12)	0.870(10)	0.007(13)
	O6	4*e*	1	0.053(11)	0.076(10)	0.421(8)	0.006(13)
	O7	4*e*	1	−0.011(12)	0.388(11)	0.349(12)	0.008(14)
b) 500 °C	Co1	4*e*	1	0.254(7)	0.944(3)	0.867(5)	0.022(11)
	Co2	4*e*	1	0.261(8)	0.562(4)	0.877(5)	0.028(14)
	P1	4*e*	1	0.488(5)	0.255(6)	0.255(6)	0.014(17)
	P2	4*e*	1	0.063(7)	0.234(8)	0.496(7)	0.016(18)
	O1	4*e*	1	0.25(2)	0.203(10)	0.650(14)	0.013(14)
	O2	4*e*	1	−0.129(18)	0.300(10)	0.527(13)	0.010(14)
	O3	4*e*	1	0.627(13)	0.253(13)	0.694(13)	0.012(14)
	O4	4*e*	1	0.520(12)	0.097(13)	0.945(11)	0.012(14)
	O5	4*e*	1	0.442(12)	0.406(12)	0.826(10)	0.013(13)
	O6	4*e*	1	0.058(10)	0.077(10)	0.390(9)	0.014(12)
	O7	4*e*	1	0.031(14)	0.371(12)	0.375(11)	0.012(13)
c) 600 °C	Co1	4*e*	1	0.262(13)	0.925(8)	0.880(8)	0.04(3)
	Co2	4*e*	1	0.257(13)	0.556(7)	0.868(7)	0.04(3)
	P1	4*e*	1	0.490(9)	0.259(18)	0.790(8)	0.02(3)
	P2	4*e*	1	0.043(11)	0.261(18)	0.474(10)	0.03(3)
	O1	4*e*	1	0.24(4)	0.21(3)	0.64(3)	0.02(5)
	O2	4*e*	1	−0.04(2)	0.22(3)	0.589(18)	0.01(5)
	O3	4*e*	1	0.661(17)	0.23(3)	0.703(11)	0.01(4)
	O4	4*e*	1	0.42(4)	0.09(3)	0.86(3)	0.02(9)
	O5	4*e*	1	0.42(4)	0.44(2)	0.82(2)	0.01(8)
	O6	4*e*	1	−0.020(18)	0.09(2)	0.344(15)	0.01(7)
	O7	4*e*	1	0.03(2)	0.42(2)	0.391(19)	0.02(6)

[*Continuing Table S24*]

Temperature	Atom	Wyck. position	Occupancy	*x*/a	*y*/b	*z*/c	U_{iso} (Å^2)
d) 700 °C	Co1	4*e*	1	0.251(10)	0.944(6)	0.872(7)	0.06(2)
	Co2	4*e*	1	0.237(11)	0.561(7)	0.870(8)	0.05(2)
	P1	4*e*	1	0.456(15)	0.272(13)	0.756(11)	0.03(4)
	P2	4*e*	1	0.039(12)	0.244(12)	0.468(8)	0.04(2)
	O1	4*e*	1	0.26(3)	0.215(15)	0.611(19)	0.04(4)
	O2	4*e*	1	−0.12(2)	0.25(2)	0.510(13)	0.02(5)
	O3	4*e*	1	0.622(13)	0.282(13)	0.685(9)	0.01(3)
	O4	4*e*	1	0.48(3)	0.10(2)	0.830(17)	0.02(6)
	O5	4*e*	1	0.41(2)	0.395(15)	0.868(16)	0.02(5)
	O6	4*e*	1	0.04(3)	0.09(3)	0.37(2)	0.02(8)
	O7	4*e*	1	0.01(2)	0.401(17)	0.360(15)	0.02(4)

[a] The estimated standard deviations were calculated by the Berar's procedure and are indicated in parentheses.

Table S25 Selected interatomic distances of α-$Co_2P_2O_7$ ($P2_1/c$, $Z = 4$) as refined from temperature-dependent *in situ* X-ray powder diffraction data at 400–700 °C [a]

	Atom pair		*d* (Å)			
			a) 400 °C	b) 500 °C	c) 600 °C	d) 700 °C
Co1	O2	×1	1.69(10)	1.95(13)	2.4(2)	2.31(19)
	O3	×1	2.17(12)	1.98(12)	2.0(2)	1.81(12)
	O4	×1	2.03(12)	1.82(8)	1.8(3)	2.2(2)
	O4	×1	2.13(9)	2.13(10)	2.5(2)	2.62(14)
	O6	×1	2.56(7)	2.46(7)	2.05(12)	2.33(18)
	O7	×1	2.21(10)	2.23(11)	2.1(2)	2.11(16)
	Co1–O average		2.13	2.10	2.14	2.2
Co2	O2	×1	2.42(9)	2.50(12)	2.2(2)	2.24(19)
	O3	×1	2.20(12)	2.00(12)	1.8(2)	2.25(13)
	O5	×1	1.83(10)	2.00(11)	1.7(3)	1.85(16)
	O6	×1	1.92(10)	1.87(9)	2.23(17)	1.9(3)
	O7	×1	2.01(9)	2.43(9)	2.41(15)	2.12(12)
	Co2–O average		2.08	2.16	2.1	2.1
P1	O1	×1	1.78(8)	1.71(11)	1.8(2)	1.53(18)
	O3	×1	1.53(12)	1.56(13)	1.71(16)	1.55(16)
	O4	×1	1.94(13)	1.87(11)	1.7(3)	1.6(2)
	O5	×1	1.59(11)	1.37(12)	1.6(3)	1.58(19)
	P1–O average		1.71	1.63	1.7	1.6
P2	O1	×1	1.62(8)	1.48(11)	1.6(2)	1.60(18)
	O2	×1	1.65(10)	1.59(15)	1.4(2)	1.35(19)
	O6	×1	1.47(9)	1.62(11)	1.8(2)	1.6(3)
	O7	×1	1.57(11)	1.54(12)	1.5(2)	1.60(17)
	P2–O average		1.58	1.56	1.6	1.5

[a] The estimated standard deviations were calculated by the Berar's procedure and are indicated in parentheses.

12 *In situ* X-ray powder diffraction patterns upon heating of $Li_{0.5-\delta}CoPO_4$ (*Cmcm*) under air at 800 °C, 900 °C, and after cooling down to room temperature (25 °C)

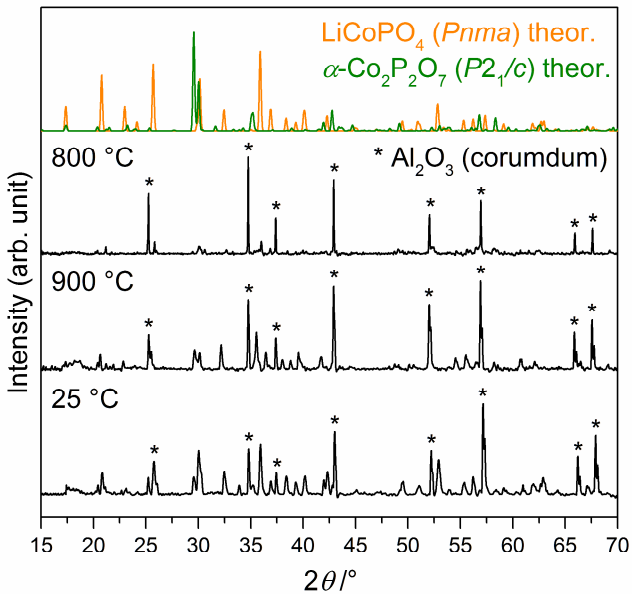

Figure S12 *In situ* X-ray powder diffraction patterns (Bragg-Brentano geometry, Cu K_α radiation) of $Li_{0.5-\delta}CoPO_4$ (*Cmcm*) measured at 800 °C and 900 °C under air (heating rate: 5 °C·min^{-1}) and after cooling to ambient temperature (25 °C). The theoretical patterns of the involved phases $LiCoPO_4$ (*Pnma*, orange, ICSD no. 431999)[2] and α-$Co_2P_2O_7$ (*P*2$_1$/*c*, green, ICSD no. 280959),[3] which were calculated from room temperature data, are displayed in color. Compared to the pattern at 700 °C (*cf.* Fig. 7 in the main article or Fig. S11i), no changes of the main phases $LiCoPO_4$ (*Pnma*) and α-$Co_2P_2O_7$ (green) is observed except for the fact that at 800 °C, strong additional reflections (marked with an asterisk *) of the corundum flat plate sample holder appear. (Since the voluminous powder showed massive shrinkage/volume reduction upon heating, the surface of the sample holder was no longer fully covered with substance at this point.)

References

1. Alarcón-Suesca, C.; Ludwig, J.; Hlukhyy, V.; Stinner, C.; Nilges, T., *Inorganics* **2016,** *4*, 35.
2. Ludwig, J.; Marino, C.; Haering, D.; Stinner, C.; Gasteiger, H. A.; Nilges, T., *J. Power Sources* **2017,** *342*, 214-223.
3. El Bali, B.; Bolte, M., *Acta Crystallogr., Sect. E: Struct. Rep. Online* **2002,** *58*, i32-i33.
4. Bramnik, N. N.; Nikolowski, K.; Baehtz, C.; Bramnik, K. G.; Ehrenberg, H., *Chem. Mater.* **2007,** *19*, 908-915.
5. Kaus, M.; Issac, I.; Heinzmann, R.; Doyle, S.; Mangold, S.; Hahn, H.; Chakravadhanula, V. S. K.; Kuebel, C.; Ehrenberg, H.; Indris, S., *J. Phys. Chem. C* **2014,** *118*, 17279-17290.
6. Kreder, K. J.; Assat, G.; Manthiram, A., *Chem. Mater.* **2015,** *27*, 5543-5549.
7. Markevich, E.; Sharabi, R.; Gottlieb, H.; Borgel, V.; Fridman, K.; Salitra, G.; Aurbach, D.; Semrau, G.; Schmidt, M. A.; Schall, N.; Bruenig, C., *Electrochem. Commun.* **2012,** *15*, 22-25.
8. Mathew, V.; Alfaruqi, M. H.; Gim, J.; Song, J.; Kim, S.; Ahn, D.; Kim, J., *Mater. Charact.* **2014,** *89*, 93-101.